Terr. Atmos. Ocean. Sci., Vol. 32, No. 6, Part II, 1093-1105, December 2021 doi: 10.3319/TAO.2021.07.28.01

Stereomic microstructure of Clypeasteroida in thin section based on new material from Pleistocene strata in Taiwan

Yu-Jou Lin[1], Jiann-Neng Fang[2], Chien-Chung Chang[3], Chi-Chieh Cheng[3], and Jih-Pai Lin[1, *]

[1] *Department of Geosciences, National Taiwan University, Taipei City, Taiwan*
[2] *Collection Management Department, National Taiwan Museum, Taipei City, Taiwan*
[3] *Delta Electronics, Inc., Taoyuan City, Taiwan*

Article history:
Received 26 March 2021
Revised 21 July 2021
Accepted 28 July 2021

Keywords:
Stereom, Echinodermata, Sand dollars, Toukoshan Formation, Quaternary geology

Citation:
Lin, Y.-J., J.-N. Fang, C.-C. Chang, C.-C. Cheng, and J.-P. Lin, 2021: Stereomic microstructure of Clypeasteroida in thin section based on new material from Pleistocene strata in Taiwan. Terr. Atmos. Ocean. Sci., 32, 1093-1105, doi: 10.3319/TAO.2021.07.28.01

ABSTRACT

The goal is to document the stereom preservation of a fossil clypeasteroid *Scaphechinus mirabilis* recovered from the Pleistocene strata in western Taiwan. The adult size of *S. mirabilis* ranges from 4 to 7 cm. Although the living species can be found along the coast in Japan, Korea, and China, only fossil materials have been reported from the Toukoshan Formation in Miaoli, Taiwan. To understand better the fossil stereom preservation of *S. mirabilis*, a total of 971 specimens deposited at the Department of Geosciences, National Taiwan University (NTUG) were examined. An additional 572 specimens were also studied and 65 well-preserved fossil specimens and one modern sample were selected for making thin sections. Among the 86 thin sections, 68 sections were prepared and cut parallel to the bilateral symmetry plane of the echinoid, and the other 18 thin sections were cut through different regions of the test, including apical system, petaloid, and interambulacral areas. Types of stereom and the associated tissues can be determined by calculating the pore size and minimum thickness of trabeculae. Results show that plate boundaries, growth lines, and stereom are clear and identifiable under a polarized microscope. Dominant types of stereom include labyrinthic, rectilinear and galleried stereom.

1. INTRODUCTION

Stereomic microstructure known as stereom is the fundamental building block of echinoderm ossicles, and they are key features to interpret the function(s) of echinoderm ossicles that originated during the Cambrian (Clausen and Smith 2005). Stereom consists of a three-dimensional mesh of trabeculae filled with interconnecting pores. Trabeculae are comprised of high-magnesium calcite, and behave as a single crystal in each ossicle (Gorzelak et al. 2016; Gorzelak 2018). At least nine types of stereom have been reported from both living and fossil echinoids (Fig. 1). Stereom studies are crucial to understand the phylogeny, growth, and soft tissue of the Echinoidea (Pearse and Pearse 1975; Seilacher 1979; Smith 1980, 1984, 1989, 1991; Ebert 2013; Grun and Nebelsick 2018a, b, c).

Fossil echinoids from Taiwan have been studied for decades, and many impressive collections are housed in both public and private museums in Taiwan. According to Lin and Chou (1978, p. 13), the earliest known report of Taiwanese fossil echinoderms was on fossil echinoids by Henry Brougham Guppy (1854 - 1926) in 1881, but the reported genus, *Scutella*, was probably misidentified (Wang 1982a). In 1885, G. A. Lebour reported two species *Echinodiscus bioculatus* Agassiz and *E. bisperforatus* Leske from Taiwan; however, those names were not considered as valid names by later authors (e.g., Yoshiwara 1901, p. 62; Hayasaka and Morishita 1947a, p. 39). During the early 20th Century, Taiwanese echinoderms were mainly studied by Japanese scholars. Yoshiwara (1903) reported three fossil echinoids from Taiwan: *Astriclypeus integer*, *Echinodiscus formosus*, and *Schizaster* sp. Deguchi (1912) listed 11 localities of fossil echinoids from Taiwan. After the end of the Second World War, echinoderm studies were resumed and led by the famous paleontologist Ichirô Hayasaka (1891 - 1977) (Hayasaka and Morishita 1947a, b; Hayasaka 1948a, b). Nisiyama (1966, 1968) reviewed and summarized previous

* *Corresponding author*
E-mail: alexjplin@ntu.edu.tw

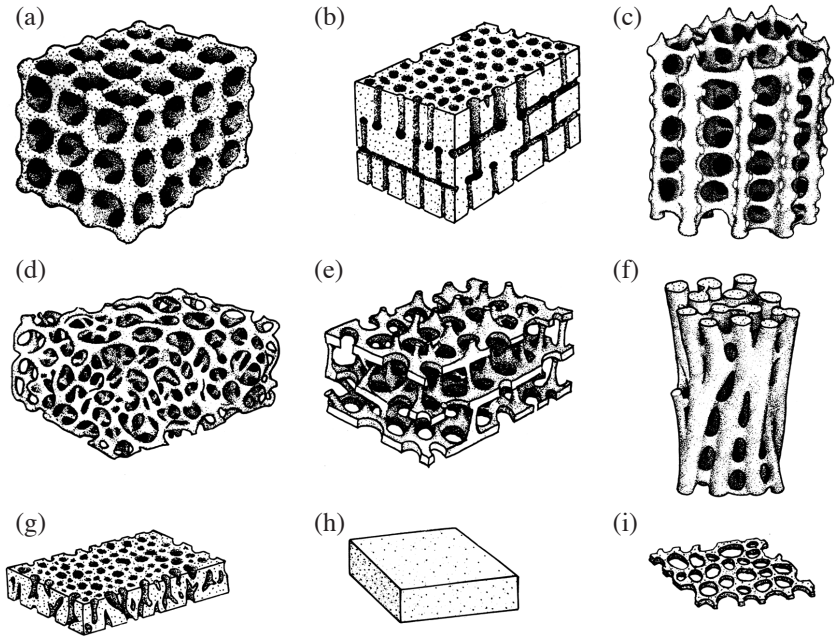

Fig. 1. Types of stereomic microstructure (stereom) (modified from Smith 1980). (a) Rectilinear; (b) microperforate; (c) galleried; (d) labyrinthic; (e) laminar; (f) fascicular; (g) perforate; (h) imperforate; (i) retiform.

studies of echinoid faunas from Japan and adjacent regions, including Taiwan. Lin and Chou (1978, p. 441 - 444) listed 11 fossil echinoid families reported from Taiwan. New findings were discovered during the field mapping project in the 1980s. This material became the core research collection of the Master's study of Chia-Ching Wang at the National Taiwan University. Wang's studies (e.g., Wang 1982a, b, 1984, 1986; Wang et al. 1984) marked an important milestone for Taiwan fossil echinoid research. By reviewing Wang's collections housed at the Department of Geosciences, National Taiwan University, new specimens are collected by re-visiting classic fossil localities. This study is a part series of reviewing and restudying Taiwanese clypeasteroids (e.g., Lee et al. 2019). The goal here is to study the stereom preservation based on *Scaphechinus mirabilis*, which is one of the most common fossil clypeasteroids recovered from the Pleistocene strata in western Taiwan (Morishita 1967; Wang et al. 1984).

2. REGIONAL GEOLOGY

Fossils are recovered from the Toukoshan Formation (Pleistocene) in Miaoli (Fig. 2), and the unit crops out in Hsinchu, Miaoli, and Taichung in western Taiwan. The unit can be divided into two members: Hsiangshan sandstone and Huoyenshan conglomerate. Fossil sand dollars commonly occur in the Hsianshan member. Based on magnetostratigraphy, the lower part of the unit belongs to the Jaramillo subchron (1.07 - 0.99 Ma) within the Matuyama Chron (Chen 2016). Chen et al. (1977) interpreted the lower boundary between Toukoshan Formation and the underlying Cholan Formation to be 1.3 Ma in age.

3. METHODOLOGY

The basic body plans of sea urchins or echinoids can be categorized into two groups: regular and irregular echinoids (Durham et al. 1966; Smith 1984; Mooi 1989). Studied materials are fossil specimens of *Scaphechinus mirabilis*, which is an irregular urchin with a bilateral symmetry. Standard terminology is explained in Fig. 3. In order to examine the marginal plates and stereom types under polarized light microscopes (PLM), the quality of thin sections is crucial.

Raw samples were cleaned, and the well-preserved fragments were selected to be trimmed down to 2 cm^2. Samples were then polished with 320-, 400-, 600-, 800-, and 1000-grit sandpapers. Samples were affixed to a glass slide with epoxy and dried in the oven for 2 hours. When the thin sections were polished to 30 μm in thickness, they were ready for PLM study (Fig. 4). Under PLM, echinoid ossicle could be recognized in both plain and polarized light (Figs. 4a, b, respectively). In order to enhance the contrast, an accessory plate (gypsum plate in this case) was inserted (Fig. 4c). Serial sections along the axial petaloid (Fig. 5a) revealed different internal features (Figs. 5c - e). When sectioned across the interporiferous zone (Figs. 5b, c), there were no supporting structures. Pillars and other supporting structures were visible in thin sections made outside of this zone (Figs. 5d, e).

For comparison sections and fragments of modern

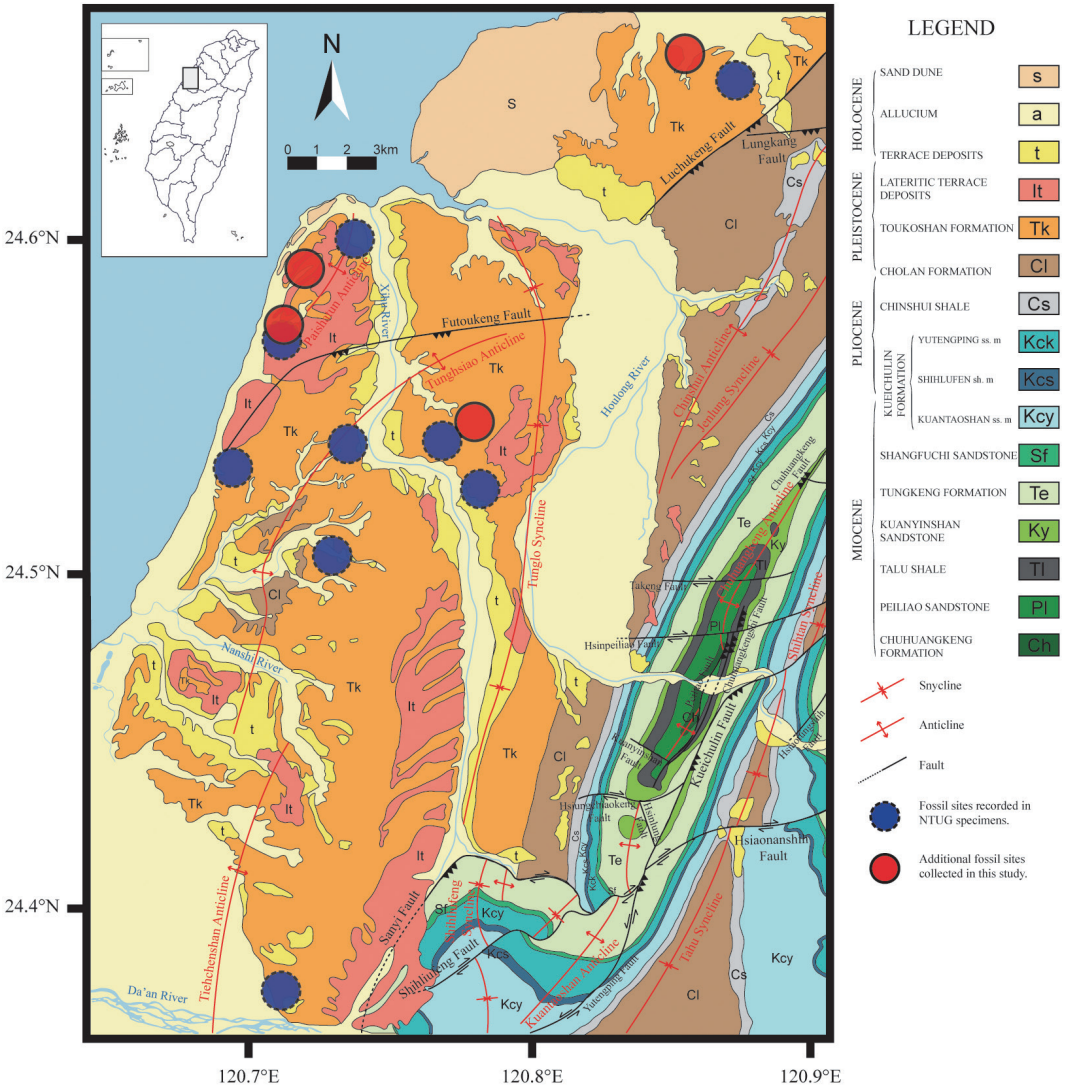

Fig. 2. Geologic map of studied area redraw from 1:50000 geologic map sheets (Paishatun, Miaoli, Tachia, and Tungshih) published by the Central Geological Survey.

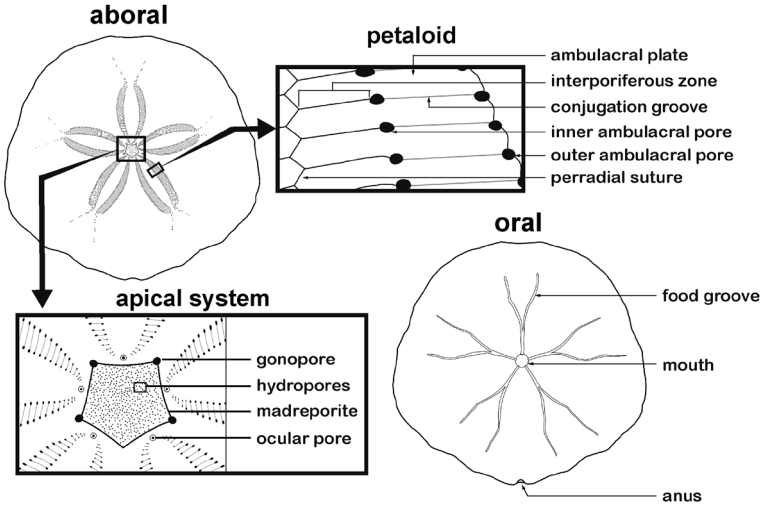

Fig. 3. Morphology of *Scaphechinus mirabilis* (modified from Lin 2021).

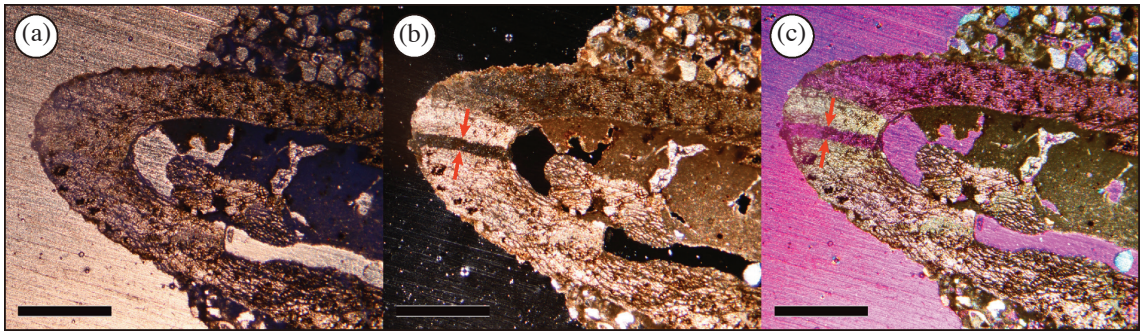

Fig. 4. Longitudinal section (NTUG300-FU01033) of *S. mirabilis* under polarized light. Scale bar = 1 mm. (a) Open nicol; (b) crossed nicols; (c) crossed nicols with a gypsum plate. Plate boundaries are marked by arrows.

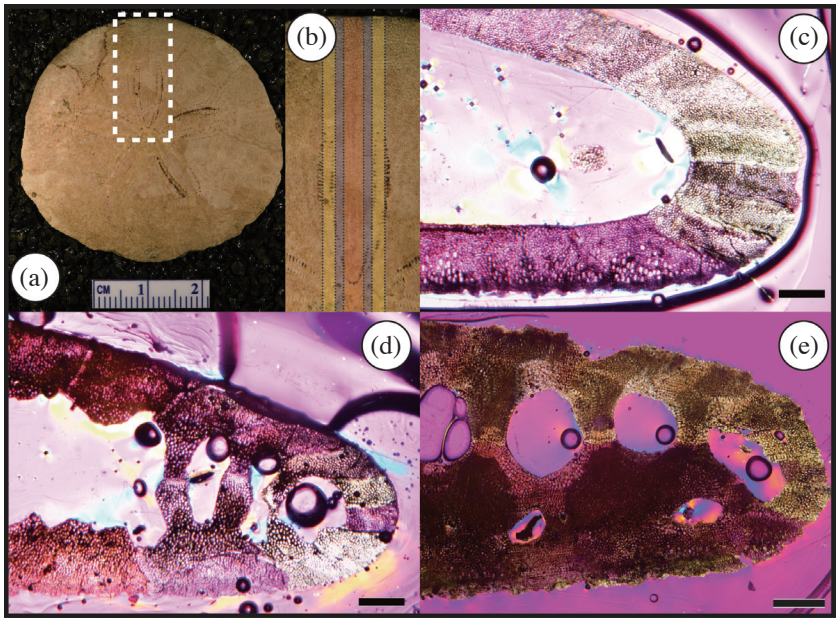

Fig. 5. Studied areas for making thin sections in different orientations. Scale bars: 0.5 cm (b) - (d). (a) A complete sample (NTUG300-FU01057) of *S. mirabilis* and the studied area (indicated by dash lines) shown in (b); (b) orientation of thin sections (NTUG300-FU01057); orange area is the target region (the interporiferous zone); yellow areas are the outer parts of petaloids; gray areas are between the two areas mentioned above; (c) sectional profile (NTUG300-FU01057) of marginal plates without pillars or supporting structures, cutting through the orange area shown in (b); (d) sectional profile (NTUG300-FU01054) of marginal plates with pillars, cutting through the gray area shown in (b); (e) sectional profile (NTUG300-FU01035) of marginal plates with dense supporting structures, cutting through the yellow area shown in (b).

specimens of *S. mirabilis* from Japan were obtained. In particular, detailed morphologic features of tubercles were examined further under the scanning electron microscope (SEM) and reported here (e.g., Figs. 6a, b, 7a, b, 8a, 9a, b, 10a, c). Well-preserved specimens were also examined under the microcomputed tomography (μCT) via DELab μCT-100X made by Delta Electronics, Inc. (Fig. 11).

Stereom was studied by measuring the average minimum diameter of trabecular thickness and the average maximum diameter of interconnecting pores. For assessing the stereom coarseness Smith (1980) divided the interconnecting pores into three levels according to their size: coarse (> 25 μm), medium (10 - 25 μm), and fine (< 10 μm). By calculating the coarseness and trabecular thickness, we calculated the stereom porosity based on the following equation:

$$\phi = \overline{A}/\overline{t} \quad (1)$$

in which, porosity (ϕ) is the average maximum diameter of interconnecting pores ($\overline{A}$) divided by the average minimum diameter of trabecular thickness ($\overline{t}$). Four degrees of stereom porosity defined in Smith (1980) were adopted here: compact ($\overline{A}/\overline{t} < 1$), dense ($2 > \overline{A}/\overline{t} > 1$), open ($4 > \overline{A}/\overline{t} > 2$), and sparse ($\overline{A}/\overline{t} > 4$) (Fig. 12).

4. RESULTS

4.1 Tubercle Stereom

Under SEM, tubercles of modern *S. mirabilis* can be subdivided into six regions (Figs. 6a, b). The center is known as the central ligament pit (I in Fig. 6b), in where the central ligament attaches to the spine. The pit is surrounded by bulbous area called mamelon (II in Fig. 6b) that is composed of imperforate stereom (Fig. 1h). Mamelon is connected to petal-like features known as crenulated platform (III in Fig. 6b) with imperforate stereom. The outer region on the raised platform below the imperforate stereom is the boss (IV in Fig. 6b) that is made out of labyrinthic stereom (Fig. 1d). There is a sharp boundary between the raised region and the adjacent concave area known as areole (V in Fig. 6b) with much larger interconnecting pores. Lastly, sometimes there is a zone with small interconnecting pores known as the scrobicular zone (VI in Fig. 6b), covering the outermost region of a tubercle. Fossil specimens are relatively less well-preserved, but the boss and areole regions can be distinguished easily, depending on the depth of the section (Figs. 6c - e).

Measurements are based on the labyrinthic stereom in both boss and areole regions. The coarseness of boss is 10.9 μm and the trabecular thickness is 12.3 μm on average. In the areole, the stereom coarseness is 18.6 μm and the trabecular thickness is 10.2 μm on average (Table 1). In general, the areole is where muscle fibres are attached; thus, the interconnecting pores are approximately 7.7 μm larger than that in the boss region, whereas the trabecular thicknesses are 2.1 μm smaller than that in the boss region (Figs. 12a, b).

4.2 Petaloid Stereom

Petaloids are characterized by the distinct pore system known as pore-pairs. Under SEM, it is evident that individual plate boundaries run through pores (Figs. 7a, b). Under polarized light, plates are elongated, parallel to the pore-pairs, and continuous to the perradial suture lines (Figs. 7c, d). Boundaries between plates do not meet symmetrically; instead, there are noticeable translocations among adjacent plates.

Petaloids are dominated by rectilinear stereom. Mean coarseness is 14.6 μm based on 55 measurements, and trabecular thickness is 12.2 μm on average based on 78 measurements. Calculated stereom porosity is 1.19, belonging to the dense grade.

4.3 Oral-Plate Stereom

Oral plates grow from the center and radiate outward with galleried stereom (Figs. 8a - c). There are solid spikes (Seilacher 1979) near the plate margins, forming trabecular interlocking-type plate boundary of Grun and Nebelsick (2018b, c). Spikes with imperforate stereom are 20.3 μm on average thickness based on 98 measurements. In the galleried stereom, the coarseness is 19.2 μm on average based on 242 measurements; the trabecular thickness is 12.2 μm on average based on 261 measurements. The calculated porosity is 1.57, belonging to the dense grade (Fig. 12c).

4.4 Lantern Stereom

Due to the relatively small opening for the peristome, the lantern is typically preserved within the test cavity of sand dollars in Taiwan. Under SEM, elements of lantern consist of branching trabeculae (Figs. 9a, b); thus, it is diagnostic for fascicular stereom (Fig. 1f). In thin sections (Fig. 9c), trabecular thickness varies; thus, meaningful measurements are not feasible. All the stereom measurements and porosity calculations are summarized in Table 1.

5. DISCUSSION

5.1 Comparisons of Modern and Fossil *S. Mirabilis*

By comparing SEM images (Figs. 6a, b) and thin sections (Fig. 10) of both modern and fossil *S. mirabilis*, it is clear that the modern sample contains more surficial features, such as detailed morphologies of tubercles (Figs. 6a, b, 10a, c). Although the fossil specimens typically have more surface abrasion, internal stereom have a little compaction and the interconnecting pores retain original geometry (Figs. 10b, d).

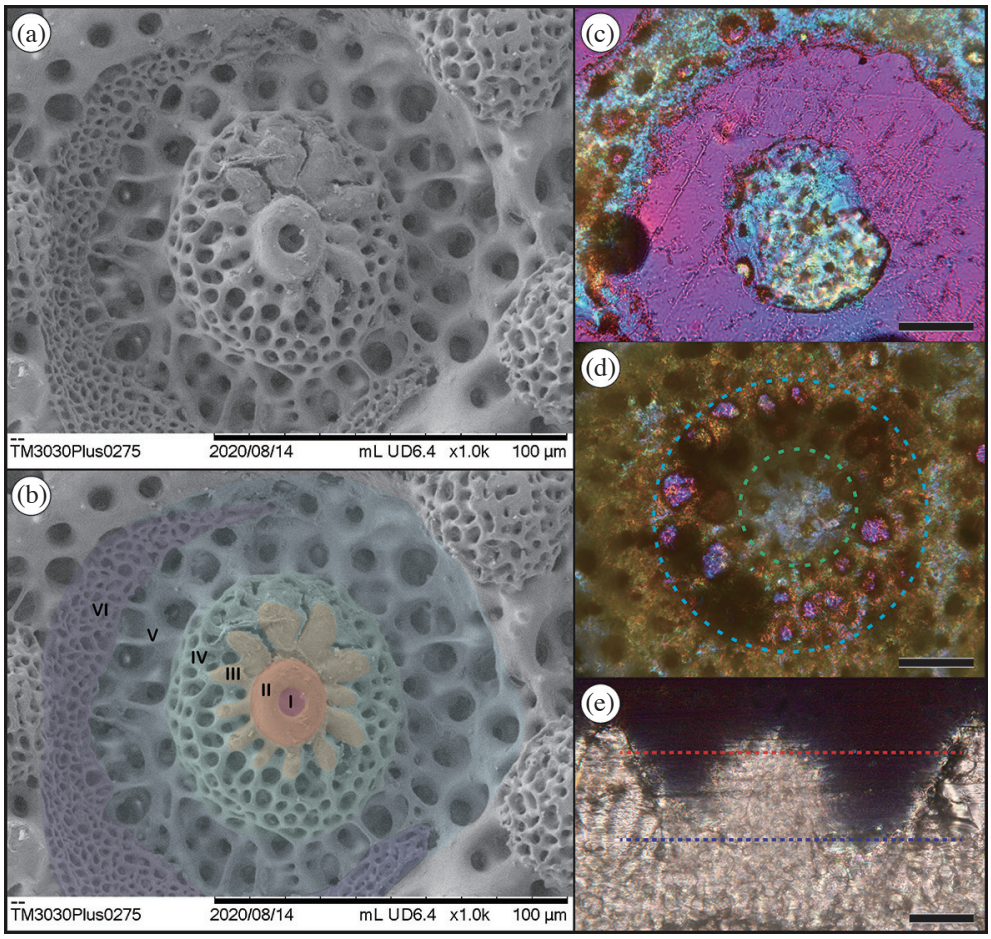

Fig. 6. Tubercle stereom under SEM (a) (b) and under polarized light microscope (PLM) (c) - (e). Scale bars: 100 µm (a) (b); 50 µm (c) - (e). (a) An original tubercle under SEM; (b) a tubercle subdivided into 6 regions that have different stereom types (I: central ligament pit, II: mamelon, III: crenulate platform, IV: boss, V: areole, VI: scrobicular zone.); (c) close-up of a tubercle highlighting mamelon and boss stereom (NTUG300-FU01067), cutting approximately through the red line illustrated in (e); (d) close-up of a tubercle highlighting boss (green dotted line region) and areole (between blue and green dotted line region) stereoms (NTUG300-FU01067), cut approximately through the blue line illustrated in (e); (e) longitudinal section (NTUG300-FU01086) of one tubercle with red and blue section surfaces presented above.

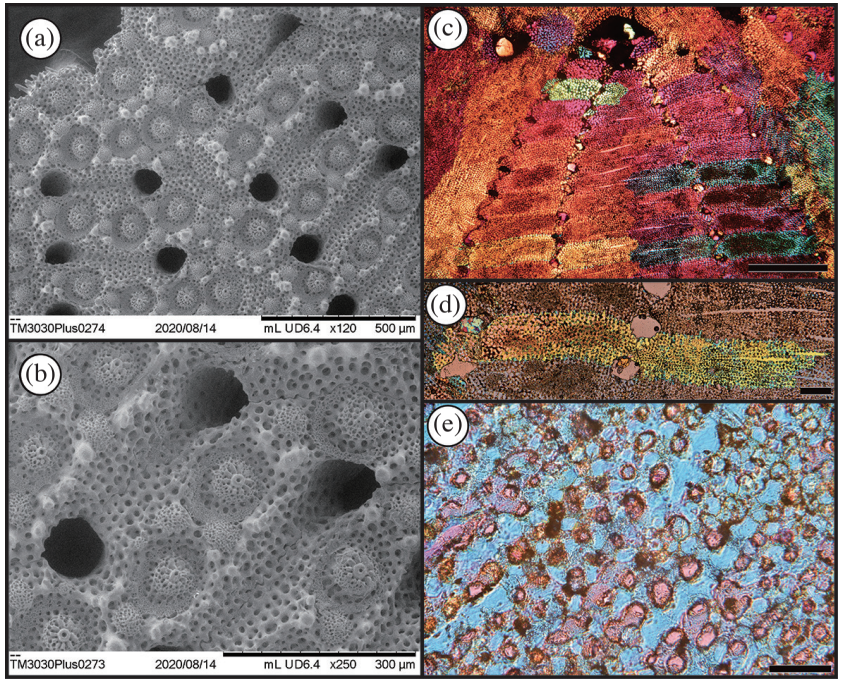

Fig. 7. Petaloid stereom under SEM (a) (b) and under PLM (NTUG300-FU01083) (c) - (e). Scale bars: 500 µm (a) (b); 1 mm (c); 200 µm (d); 50 µm (e). (a) Pairs of ambulacral pores under SEM; (b) close-up of one pore-pair; (c) partial petaloid near apical system; (d) yellow part of a petaloid belongs a single plate; (e) stereom of a petaloid.

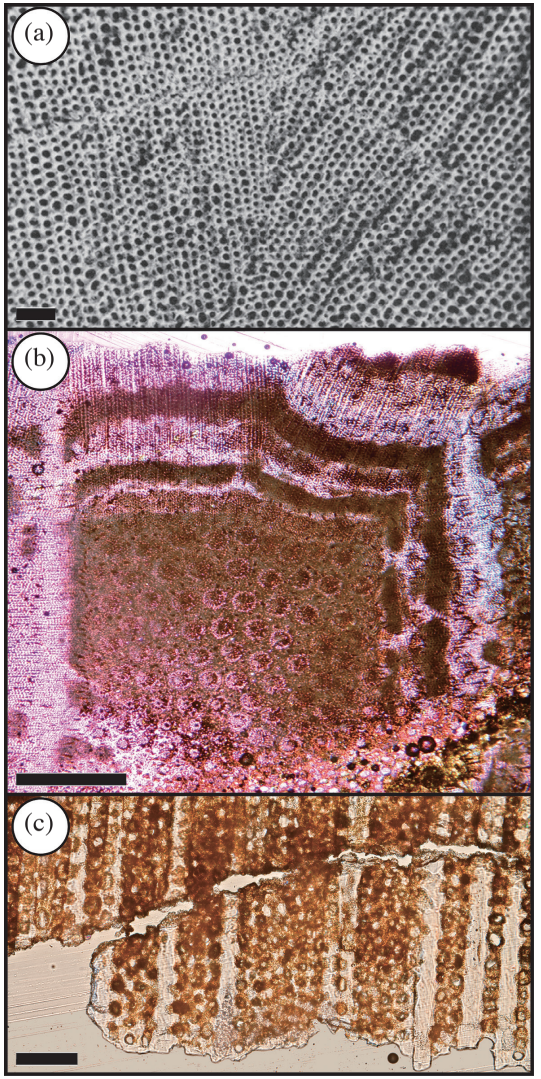

Fig. 8. Oral-plate stereom under SEM (a) and under PLM (b) (c). Scale bars: 100 µm (a) (c); 1 mm (b). (a) Oral-plate of *Clypeaster subdepressus* under SEM (modified from Seilacher 1979, Fig. 10c); (b) oral-plate (NTUG300-FU01067) of *S. mirabilis*; (c) example of galleried stereom (NTUG300-FU01074) in *S. mirabilis*.

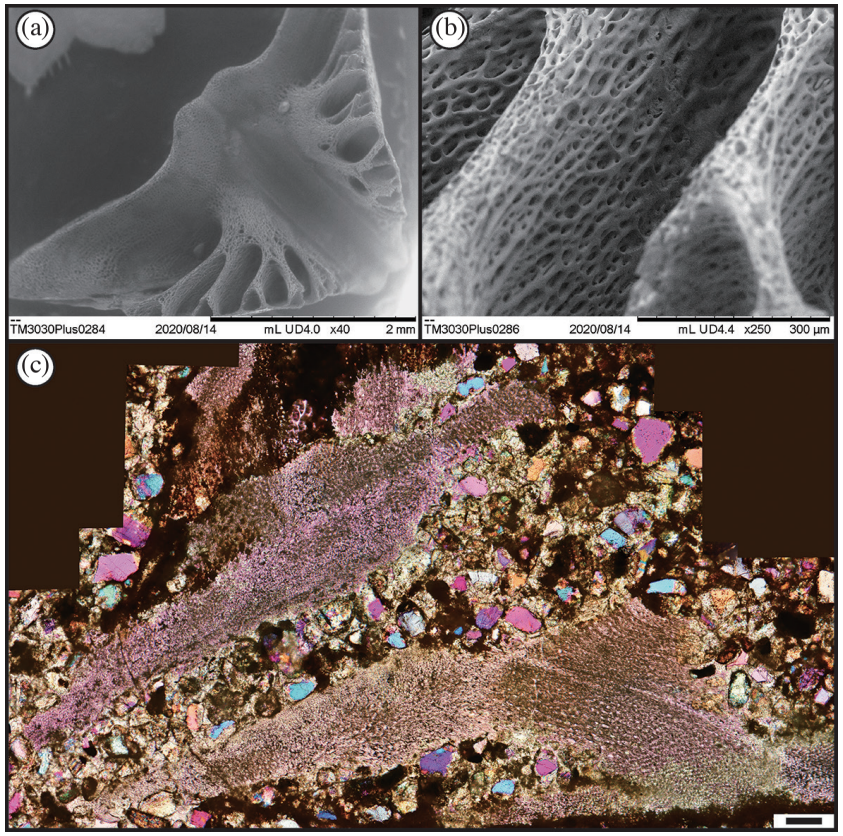

Fig. 9. Teeth stereom under SEM (a) (b) and under PLM (c). Scale bars: 2 mm (a); 300 µm (b); 200 µm (c). (a) Lantern elements of modern *S. mirabilis* under SEM; (b) close-up of (a) showing the bifurcated stereom, which is indicative of fascicular stereom; (c) thin section (NTUG300-FU01075) of fossil *S. mirabilis* containing the lantern (in tangential view).

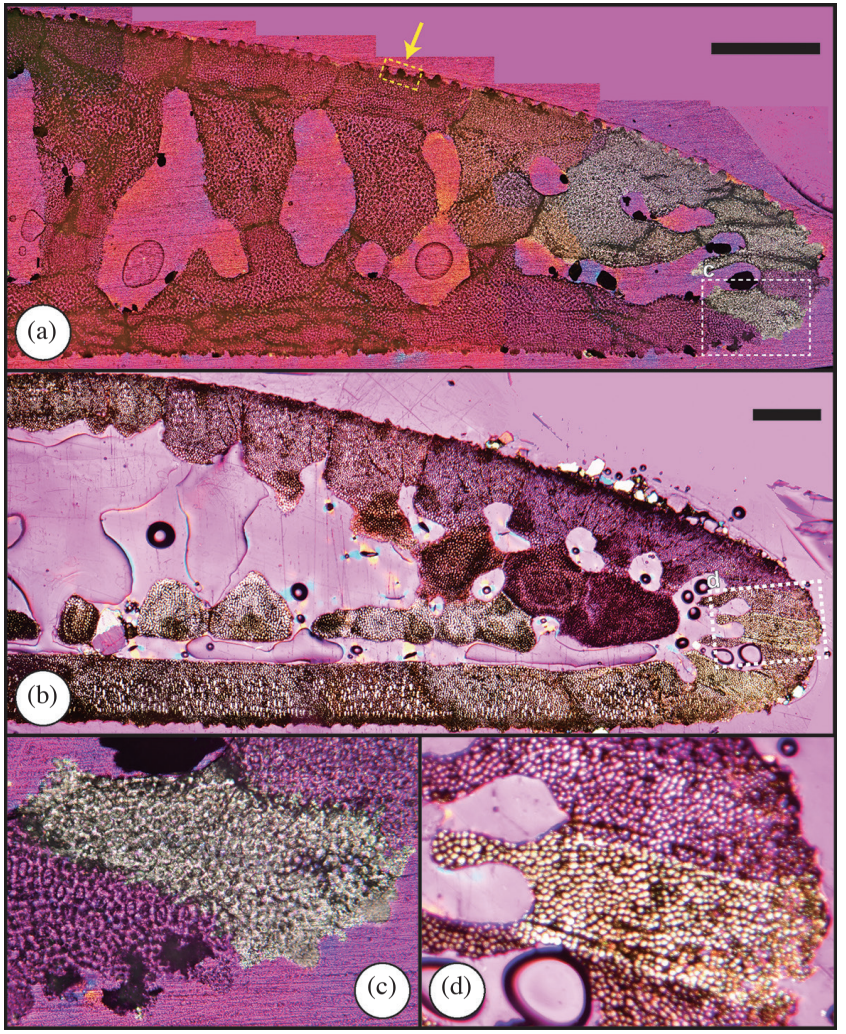

Fig. 10. Comparison of fossil (a) (c) and modern (b) (d) *S. mirabilis* thin sections under PLM. Scale bars: 1 mm (a) (b). (a) Thin section (NTUG300-FU01086) of a modern *S. mirabilis*. Tubercles are indicated by a yellow arrow; (b) Thin section (NTUG300-FU01064) of a fossil *S. mirabilis*; (c) close-up of the dotted rectangle indicated in (a); (d) close-up of the dotted region indicated in (b).

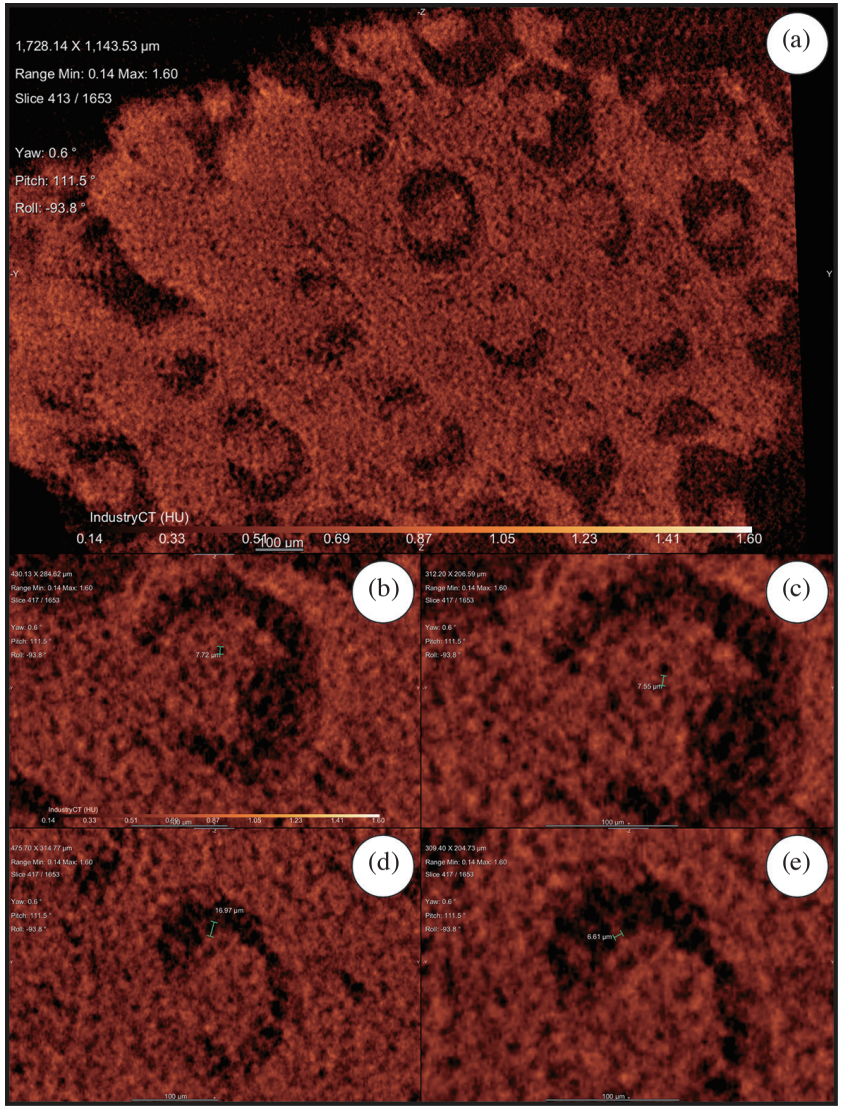

Fig. 11. µCT imaging of a section of tubercles on the oral surface with Delta µCT-100X. (a) Reconstructed *S. mirabilis* virtual plates; (b) measurement of the representative interconnecting pore in the boss region within a tubercle; (c) measurement of the representative trabecular thickness in the boss region within a tubercle; (d) measurement of the representative interconnecting pore in the areole region within a tubercle; (e) measurement of the representative trabecular thickness in the areole region within a tubercle.

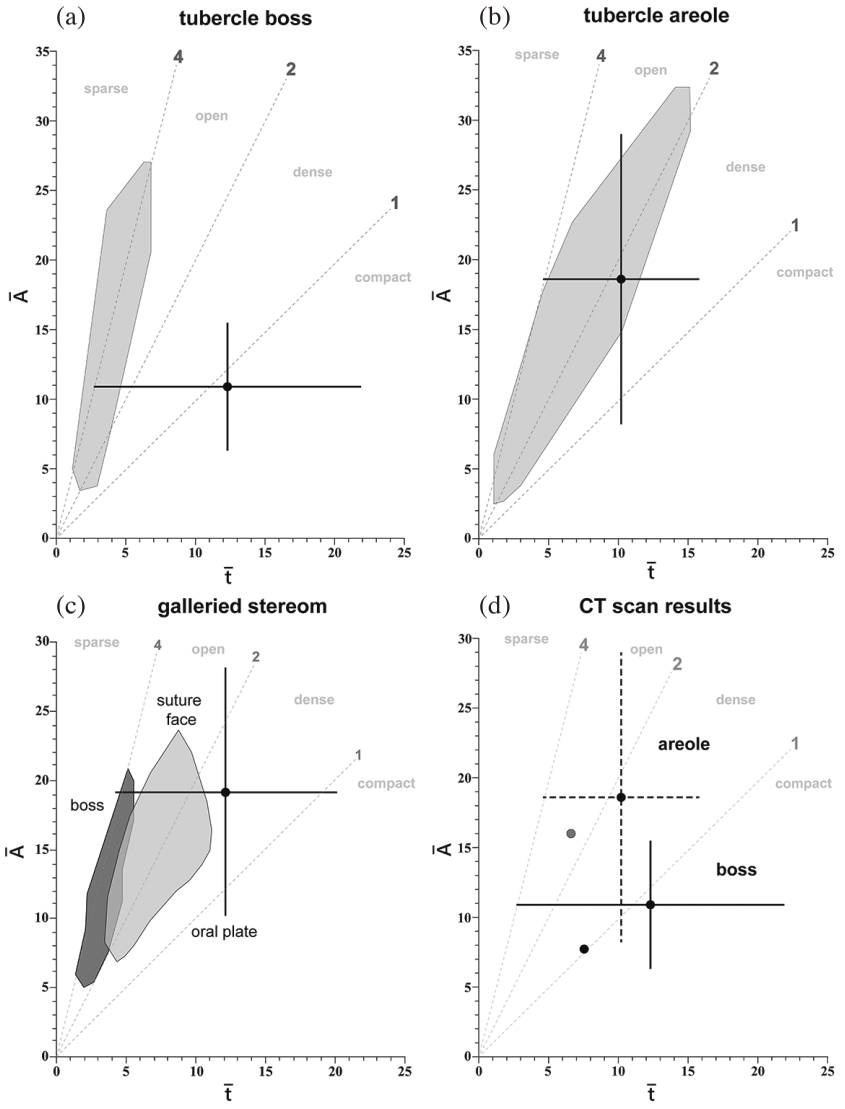

Fig. 12. Plots of fossil *S. mirabilis* stereom measurements (solid lines and dashed lines) compared with 32 living echinoids in Smith (1980). Dotted lines are boundaries of stereom coarseness defined in Smith (1980). Solid regions are known echinoderm stereom types defined in Smith (1980). Solid lines represent the mean ±2 standard deviations for *S. mirabilis* stereom measured in this study. (a) Boss stereom measurements compared to Smith (1980); (b) areole stereom measurements compared to Smith (1980); (c) galleried stereom measurements compared to Smith (1980); (d) areole and boss stereom measurements (dashed lines and solid lines) compared to µCT imaging results (grey circle and black circle).

Table 1. Summary of stereom measurements based on fossil *S. mirabilis* from Taiwan.

	Boss	**Areole**	**Petaloid**	**Oral plate**
Stereom type	Labyrinthic	Labyrinthic	Rectilinear	Galleried
Mean pore diameter	10.9 μm (n = 52)	18.6 μm (n = 130)	14.6 μm (n = 55)	19.2 μm (n = 242)
Trabecular thickness	12.3 μm (n = 78)	10.2 μm (n =159)	12.2 μm (n = 78)	12.2 μm (n = 261)
Porosity	0.9	1.8	1.2	1.6
	compact	dense	dense	dense

Interconnecting pores are where soft tissues attached; thus, there are commonly stained by dark materials in fossil specimens. In contrast, the trabeculae are translucent and retain their optical properties. In particular, individual plate still behaves as single high-Mg calcite (Towe 1967; Weber 1969; Smith 1989; Davies and John 2019) and exhibits uniaxial extinction under PLM.

5.2 μCT Imaging

μCT imaging is a non-destructive technique to visualize fossil urchins based on X-ray (Grun and Nebelsick 2018a). With the μCT-100X, the main advantage is that virtual thin-slices in any angles are possible based on the computed three-dimensional reconstruction, allowing a detailed comparison with images of our thin sections. A well-preserved fragment was tested with this method, and our initial findings include the following. First, the image is monotone and only the dense calcite materials can be preserved, and the interconnecting pores are left empty. This makes the distinctions between the trabeculae and interconnecting pore space much easier. Second, due to the high imaging resolution (~1 μm) the measurements are more precise than those based on optical microscope images. For example, the boss trabeculae are 7.55 μm in minimum thickness, the interconnecting pore is 7.72 μm in size, areole trabeculae are 6.61 μm in minimum thickness, and the interconnecting pore is 16.97 μm (Figs. 11, 12d) in size.

6. CONCLUSION

(1) Because fossil specimens are so well-preserved that trabeculae still behave as a single crystal for each ossicle. Under PLM, plate boundaries can be identified clearly and several types of microstructure, including rectilinear, galleried, and labyrinthic stereoms, can be measured (Table 1) and documented.
(2) Boss region consists of labyrinthic stereom. The mean pore diameter of the boss region within a tubercle is 10.9 μm based on 52 measurements, and the average trabecular thickness is 12.3 μm based on 78 measurements. The porosity of tubercle boss is compact (0.9; Table 1). Observed results of trabecular thickness based on thin sections seem to be larger than those reported in Smith (1980).
(3) Areole region is comprised of labyrinthic stereom. The mean pore diameter of the areole region within a tubercle is 18.6 μm based on 130 measurements, and the average trabecular thickness is 10.2 μm based on 159 measurements. Porosity of tubercle areole is dense (1.8; Table 1). Areole is the place where spine muscles are attached, so both the mean pore diameter and porosity are larger than that of boss.
(4) Petaloid is dominated by rectilinear stereom. The mean pore diameter of petaloid is 14.6 μm based on 55 measurements, and the average trabecular thickness is 12.2 μm based on 78 measurements. The porosity of petaloid stereom is dense (1.2; Table 1).
(5) Oral plate is dominated by galleried stereom. The mean pore diameter is 19.2 μm based on 242 measurements, and the average trabecular thickness is 12.2 μm based on 261 measurements. The porosity of galleried stereom in oral plates is dense (1.6; Table 1).
(6) On the margins of oral plates, some spike-like trabeculae, penetrating into adjacent plates are present. The average trabecular thickness of these spikes is 20.3 μm based on 98 measurements.
(7) Measurements based virtual reconstructions of μCT-100X images fit within the ranges of our results derived from thin sections.

Acknowledgements Special thanks to Chia-Hsiang Wang for donating some studied fossil specimens; Wei-Chia Chu for accessing the SEM instrument; Satoshi Takeda for donating living specimens for comparison; Min-Yuan Tseng for arranging the visit to use the μCT-100X machine in the Delta factory. This study was funded by Taiwan Ministry of Science and Technology (MOST 108-2116-M-002-014; MOST 109-2116-M-002-020; and MOST 110-2116-M-002-016 to JPL).

REFERENCES

Chen, P.-H., T.-C. Huang, C.-Y. Huang, M.-J. Jiang, S.-L. Lo, and C.-L. Kuo, 1977: Paleomagnetic and coccolith stratigraphy of Plio-Pleistocene shallow marine

sediments, Chuhuangkeng, Miaoli. *Petrol. Geol. Taiwan*, **14**, 219-239.

Chen, W.-S., 2016: Introduction to Geology of Taiwan, Geological Society of Taiwan, Taipei, Taiwan, 204 pp. (in Chinese)

Clausen, S. and A. B. Smith, 2005: Palaeoanatomy and biological affinities of a Cambrian deuterostome (Stylophora). *Nature*, **438**, 351-354, doi: 10.1038/nature04109. [Link]

Davies, A. J. and C. M. John, 2019: The clumped (^{13}C—^{18}O) isotope composition of echinoid calcite: Further evidence for "vital effects" in the clumped isotope proxy. *Geochim. Cosmochim. Acta*, **245**, 172-189, doi: 10.1016/j.gca.2018.07.038. [Link]

Deguchi, Y., 1912: Catalogue of fossils from Formosa. *The Journal of the Geological Society of Japan*, **19**, 419-428. (in Japanese)

Durham, J. W., H. B. Fell, A. G. Fischer, P. M. Kier, R. V. Melville, D. L. Pawson, and C. D. Wagner, 1966: Echinoids. In: Moore, R. C. (Ed.), Treatise on Invertebrate Paleontology, Part U: Echinodermata 3, Vol. 1 & 2, The Geological Society of America, Inc. and The University of Kansas Press, Boulder and Lawrence, U211-U640.

Ebert, T. A., 2013: Growth and survival of postsettlement sea urchins. In: Lawrence, J. M. (Ed.), Sea Urchins: Biology and Ecology, Developments in Aquaculture and Fisheries Science, Volume 38, Elsevier, 83-117, doi: 10.1016/B978-0-12-396491-5.00007-1. [Link]

Gorzelak, P., 2018: Microstructural evidence for stalk autotomy in *Holocrinus* – The oldest stem-group isocrinid. *Palaeogeogr. Palaeoclimatol. Palaeoecol.*, **506**, 202-207, doi: 10.1016/j.palaeo.2018.06.036. [Link]

Gorzelak, P., T. Krzykawski, and J. Stolarski, 2016: Diagenesis of echinoderm skeletons: Constraints on paleoseawater Mg/Ca reconstructions. *Global Planet. Change*, **144**, 142-157, doi: 10.1016/j.gloplacha.2016.07.010. [Link]

Grun, T. B. and J. H. Nebelsick, 2018a: Structural design of the echinoid's trabecular system. *PLOS ONE*, **13**, e0204432, doi: 10.1371/journal.pone.0204432. [Link]

Grun, T. B. and J. H. Nebelsick, 2018b: Structural design of the minute clypeasteroid echinoid *Echinocyamus pusillus*. *R. Soc. Open Sci.*, **5**, 171323, doi: 10.1098/rsos.171323. [Link]

Grun, T. B. and J. H. Nebelsick, 2018c: Technical biology of the clypeasteroid echinoid *Echinocyamus pusillus*: A review. *Contemp. Trends. Geosci.*, **7**, 247-254. Available at https://www.kgs.wnoz.us.edu.pl/ctg/ctg-archive/ctg-2018-7-2/.

Hayasaka, I., 1948a: Notes on some fossil echinoids of Taiwan, III. *Acta Geol. Taiwan.*, **1**, 111-128.

Hayasaka, I., 1948b: Notes on some fossil echinoids of Taiwan, IV. *Acta Geol. Taiwan.*, **2**, 85-124.

Hayasaka, I. and A. Morishita, 1947a: Fossil species of *Clypeaster* from Taiwan. *Acta Geol. Taiwan.*, **1**, 39-52.

Hayasaka, I. and A. Morishita, 1947b: Notes on some fossil echinoids of Taiwan, II. *Acta Geol. Taiwan.*, **1**, 93-109.

Lee, H., J.-P. Lin, H.-C. Li, L.-Y. Chang, K.-S. Lee, S.-J. Lee, W.-J. Chen, A. Sankar, and S.-C. Kang, 2019: Young colonization history of a widespread sand dollar (Echinodermata; Clypeasteroida) in western Taiwan. *Quat. Int.*, **528**, 120-129, doi: 10.1016/j.quaint.2018.12.003. [Link]

Lin, C. C. and J. T. Chou, 1978: Geology of Taiwan, Mao-Chang Books Co. Ltd., Taipei, Taiwan, 450 pp. (in Chinese)

Lin, Y. J., 2021: Ontogenetic Patterns and Stereomic Microstructures in Clypeasteroida: A Case Study of Pleistocene Sand Dollars from Western Taiwan. Mater Thesis, National Taiwan University, Taipei, Taiwan, 91 pp.

Mooi, R., 1989: Living and Fossil Genera of the Clypeasteroida (Echinoidea: Echinodermata): An Illustrated Key and Annotated Checklist, Smithsonian Contributions to Zoology, Number 488, 51 pp, doi: 10.5479/si.00810282.488. [Link]

Morishita, A., 1967: On the measurements of *Scaphechinus mirabilis* (preliminary report). Contributions to Celebrate Prof. Ichiro Hayasaka's 76th Birthday, 109-116.

Nisiyama, S., 1966: The Echinoid Fauna from Japan and Adjacent Regions: Part 1, Palaeontological Society of Japan Special Papers, Number 11, 277 pp.

Nisiyama, S., 1968: The Echinoid Fauna from Japan and Adjacent Regions: Part 2, Palaeontological Society of Japan Special Papers, Number 13, 491 pp.

Pearse, J. S. and V. B. Pearse, 1975: Growth Zones in the Echinoid Skeleton. *Am. Zool.*, **15**, 731-751, doi: 10.1093/icb/15.3.731. [Link]

Seilacher, A., 1979: Constructional morphology of sand dollars. *Paleobiology*, **5**, 191-221, doi: 10.1017/S0094837300006527. [Link]

Smith, A. B., 1980: Stereom Microstructure of the Echinoid Test, Special Papers in Palaeontology, Vol. 25, Palaeontological Association, 81 pp.

Smith, A. B., 1984: Echinoid Palaeobiology, Special Topics in Palaeontology, Vol. 1, George Allen and Unwin, London, 190 pp.

Smith, A. B., 1989: Biomineralization in Echinoderms. In: Carter, J. G. (Ed.), Skeletal Biomineralization: Patterns, Processes and Evolutionary Trends, Short Courses in Geology, Volume 5, American Geophysical Union, 117-147, doi: 10.1029/SC005p0117. [Link]

Smith, A. B., 1991: Echinodermata Plates 170-175. In: Carter, J. G. (Ed.), Skeletal Biomineralization: Patterns, Processes and Evolutionary Trends, Volume II, Atlas and Index, Van Nostrand Reinhold, New York, 69-71.

Towe, K. M., 1967: Echinoderm calcite: Single crystal or

polycrystalline aggregate. *Science*, **157**, 1048-1050, doi: 10.1126/science.157.3792.1048. [Link]

Wang, C.-C., 1982a: Study on fossil clypeasteroid echinoids of Taiwan. Master Thesis, Geological Department, National Taiwan University, Taipei, Taiwan, 173 pp.

Wang, C.-C., 1982b: On the fossil laganid echinoids from Taiwan, with a discussion of the "genus" *Peronellites* Hayasaka and Morishita. *Science Reports of the National Taiwan University ACTA Geologica Taiwanica*, **21**, 140-156.

Wang, C.-C., 1984: New classification of clypeasteroid echinoids. *Proc. Geol. Soc. China*, **27**, 119-152.

Wang, C.-C., 1986: Fossil astriclypeid echinoids from Taiwan. *Proc. Geol. Soc. China*, **29**, 149-183.

Wang, C.-C., C.-F. Lin, and L.-C. Lee, 1984: Measurements on Late Pleistocene sand dollar *Scaphechinus mirabilis* from northern Taiwan. *Annual Report of Central Geological Survey*, **72**, 49-56. (in Chinese)

Weber, J. N., 1969: The incorporation of magnesium into the skeletal calcites of echinoderms. *Am. J. Sci.*, **267**, 537-566, doi: 10.2475/ajs.267.5.537. [Link]

Yoshiwara, S., 1901: Geologic structure of the Riukiu Loochoo curve, and its relation to the northern part of Formosa. *The Journal of the College of Science, Imperial University of Tokyo, Japan*, **16**, 1-67.

Yoshiwara, S., 1903: On the fossil echinoids of Japan. *The Journal of the College of Science, Imperial University of Tokyo, Japan*, **17**, 1-27.

APPENDIX

Table A1. List of thin sections in Lin (2021).

NTUG No.	Specimen No.	Thin section no.	Collection	NTUG No.	Specimen No.	Thin section no.	Collection
NTUG300-FU01001	NTU1	NTU1	R300	NTUG300-FU01030	NTU47	NTU47	R300
NTUG300-FU01002	NTU2	NTU2	R300	NTUG300-FU01031	NTU48	NTU48	R300
NTUG300-FU01003	NTU3	NTU3	R300	NTUG300-FU01032	NTU49	NTU49	R300
NTUG300-FU01004	NTU4	NTU4	R300	NTUG300-FU01033	NTU50	NTU50	R300
NTUG300-FU01005	NTU5	NTU5	R300	NTUG300-FU01034	P1	P1	R111
NTUG300-FU01006	NTU6	NTU6	R300	NTUG300-FU01035	P2	P2	R111
NTUG300-FU01007	NTU7	NTU7	R300	NTUG300-FU01036	P3	P3	R111
NTUG300-FU01008	NTU8	NTU8	R300	NTUG300-FU01037	P4	P4	R111
NTUG300-FU01009	NTU9	NTU9	R300	NTUG300-FU01038	P5	P5	R111
NTUG300-FU01010	NTU10	NTU10	R300	NTUG300-FU01039	P6	P6	R111
NTUG300-FU01011	NTU11	NTU11	R300	NTUG300-FU01040	P7	P7	R111
NTUG300-FU01012	NTU12	NTU12	R300	NTUG300-FU01041	P8	P8	R111
NTUG300-FU01013	NTU13	NTU13	R300	NTUG300-FU01042	P9	P9	R111
NTUG300-FU01014	NTU14	NTU14	R300	NTUG300-FU01043	P10	P10	R111
NTUG300-FU01015	NTU15	NTU15	R300	NTUG300-FU01044	P11	P11	R111
NTUG300-FU01016	NTU16	NTU16	R300	NTUG300-FU01045	P12	P12	R111
NTUG300-FU01017	NTU17	NTU17	R300	NTUG300-FU01046	P13	P13	R111
NTUG300-FU01018	NTU18	NTU18	R300	NTUG300-FU01047	P14	P14	R111
NTUG300-FU01019	NTU19	NTU19	R300	NTUG300-FU01048	P15	P15	R111
NTUG300-FU01020	NTU20	NTU20	R300	NTUG300-FU01049	P16	P16	R111
NTUG300-FU01021	NTU21	NTU21	R300	NTUG300-FU01050	P17	P17	R111
NTUG300-FU01022	NTU22	NTU22	R300	NTUG300-FU01051	P18	P18-1	R111
NTUG300-FU01023	NTU23	NTU23	R300	NTUG300-FU01052	P18	P18-2	R111
NTUG300-FU01024	NTU24	NTU24	R300	NTUG300-FU01053	P19	P19	R111
NTUG300-FU01025	NTU25	NTU25	R300	NTUG300-FU01054	P20	P20	R111
NTUG300-FU01026	NTU42	NTU42	R300	NTUG300-FU01055	P21	P21	R111
NTUG300-FU01027	NTU43	NTU43	R300	NTUG300-FU01056	P22	P22	R111
NTUG300-FU01028	NTU45	NTU45	R300	NTUG300-FU01057	P23	P23	R111
NTUG300-FU01029	NTU46	NTU46	R300	NTUG300-FU01058	P24	P24	R111

*Note: * = modern S. mirabilis, indicates a modern specimen from Japan.*

Table A1. (Continued)

NTUG No.	Specimen No.	Thin section no.	Collection	NTUG No.	Specimen No.	Thin section no.	Collection
NTUG300-FU01059	P25	P25	R111	NTUG300-FU01073	a4	a4-2	R111
NTUG300-FU01060	P26	P26	R111	NTUG300-FU01074	a4	a4-3	R111
NTUG300-FU01061	P27	P27	R111	NTUG300-FU01075	a5	a5	R111
NTUG300-FU01062	P28	P28	R111	NTUG300-FU01076	a6	a6	R111
NTUG300-FU01063	P29	P29	R111	NTUG300-FU01077	a6	a6-2	R111
NTUG300-FU01064	P30	P30	R111	NTUG300-FU01078	a6	a6-3	R111
NTUG300-FU01065	P31	P31	R111	NTUG300-FU01079	a7	a7	R111
NTUG300-FU01066	P32	P32	R111	NTUG300-FU01080	a8	a8-1	R111
NTUG300-FU01067	T1	T1	R111	NTUG300-FU01081	a8	a8-2	R111
NTUG300-FU01068	T2	T2	R111	NTUG300-FU01082	a8	a8-3	R111
NTUG300-FU01069	T3	T3	R111	NTUG300-FU01083	a9	a9-1	R111
NTUG300-FU01070	a2	a2-1	R111	NTUG300-FU01084	a9	a9-2	R111
NTUG300-FU01071	a2	a2-2	R111	NTUG300-FU01085	a13	a13	R111
NTUG300-FU01072	a4	a4-1	R111	NTUG300-FU01086	SM016*	SM016*	R111